



The Society shall not be responsible for statements or opinions advanced in papers or discussion at meetings of the Society or of its Divisions or Sections, or printed in its publications. Discussion is printed only if the paper is published in an ASME Journal. Authorization to photocopy for internal or personal use is granted to libraries and other users registered with the Copyright Clearance Center (CCC) provided \$3/article is paid to CCC, 222 Rosewood Dr., Danvers, MA 01923. Requests for special permission or bulk reproduction should be addressed to the ASME Technical Publishing Department.

Copyright © 1999 by ASME

All Rights Reserved

Printed in U.S.A.



TURBINE NOZZLE FILM COOLING STUDY USING THE PRESSURE SENSITIVE PAINT (PSP) TECHNIQUE

Luzeng Zhang, Michael Baltz, Ram Pudupatty and Michael Fox

Solar Turbines Incorporated
P. O. Box 85376
San Diego, CA 92186-5376
U.S.A.

ABSTRACT

The use of pressure sensitive paint (PSP) to measure film cooling effectiveness on a turbine nozzle surface was demonstrated in a high speed wind tunnel. Film cooling effectiveness was measured from a single row of holes located on a turbine vane suction surface with a shaped exit. Nitrogen gas was used to simulate film cooling flow as well as a tracer gas to indicate oxygen concentration such that film effectiveness by the mass transfer analogy could be obtained. Three blowing ratios were studied for each of the five freestream conditions: a reference condition, a reduced and an increased Reynolds number condition, and a reduced and an increased Mach number condition. The freestream turbulence intensity was kept at 12.0% for all the tests. The PSP was calibrated at various temperatures and pressures to obtain better accuracy before being applied to the airfoil surface. The film effectiveness increased with blowing ratio for all the freestream conditions. The effects of secondary flow and freestream Mach number and Reynolds number on turbine nozzle suction surface film cooling are also discussed.

NOMENCLATURE

Symbols

C	chord length, cm
D	film hole diameter, cm
I	light intensity
Lu	turbulence energy length scale, cm
m	mass flow rate, kg/s
M	blowing ratio, $\rho_c V_c / \rho_\infty V_\infty$
p	pressure, kPa
P	pitch value between film holes, cm
PSP	pressure sensitive paint
SS	suction surface
T	temperature, °K
Tu	turbulence intensity
V	velocity, m/s
X	stream wise distance, cm

Y	span wise distance, cm
η	film effectiveness
μ	dynamic viscosity, Ns/m ²
ρ	density, kg/m ³
Λ_f	turbulence integral length scale, cm

Subscripts

1	cascade inlet
2	cascade exit
c	coolant condition
o	reference condition
∞	freestream condition
mix	mixture condition

INTRODUCTION

Discrete-hole film cooling is an effective method of reducing the heat load to a turbine airfoil and, when combined with internal cooling, meets the airfoil cooling requirements. As gas turbine efficiency and performance are getting higher, combustor exit temperature increases, and the demand on film cooling air heightens. To optimize film cooling design, a better understanding of film cooling physics is always in need. As discussed by Goldstein (1971), the reference temperature for calculating film cooling is usually the adiabatic wall temperature T_{aw} . This temperature is usually reported in non-dimensional form as the adiabatic film effectiveness η .

$$\eta = \frac{T_{aw} - T_\infty}{T_c - T_\infty} \quad (1)$$

T_∞ is the hot gas temperature, and T_c is the coolant temperature. While both η and the heat transfer coefficient h must be known to calculate the heat transfer, this study will focus on a technique to obtain η .

Due to difficulties associated with numerically obtaining film effectiveness, an extensive effort has been made to obtain it

experimentally. The turbine airfoil film cooling measurement is characterized by the airfoil geometry and the complexity of the flow field and operating parameters. Various experimental methodologies have been employed to obtain the film effectiveness and the heat transfer coefficients from a turbine airfoil surface. Among others, Takeishi et al. (1989) performed film cooling measurements on turbine nozzle pressure and suction surfaces with double row injection using thin film heater and thermocouple techniques. On the suction surface, the film effectiveness at the 83% span dropped quickly compared to those at the mid-span due to the secondary flow effect. A similar method was used by Ames (1997a, 1997b) to obtain both the film effectiveness and the heat transfer coefficient from a linear turbine nozzle cascade. The effect of turbulence intensity and pressure gradient was studied. Though the tests were performed at multiple Reynolds numbers, the effect of Reynolds number on film cooling was not clearly indicated. A slightly different approach was employed by Abuaf et al. (1995). The film effectiveness and the heat transfer coefficient were measured from a turbine nozzle surface using steady-state and transient mode testing on a thermocouple instrumented nozzle airfoil in a high speed cascade. Another traditional method to measure the film effectiveness is the tracer gas/gas chromatography technique (Goldstein, 1971 or Pederson, 1977). Using this method, Takeishi et al. (1991) measured film effectiveness from a rotating rotor blade in a air turbine. On both the pressure and the suction surface, the film effectiveness decreased quickly in the streamwise direction. Recently, the transient liquid crystal technique has been used to obtain the film effectiveness and the heat transfer coefficient (Vedula and Metzger, 1991; Wang et al., 1994). Recently, Du et al. (1997) studied the unsteady wake effect on turbine blade film cooling using the transient liquid crystal technique. They indicated that under unsteady wake conditions, the film effectiveness increased with blowing ratio for shaped hole injection. Drost and Böls (1998) performed detailed film cooling measurement on a turbine airfoil surface through single and double injection using the transient liquid crystal technique. Considering only the suction surface results, for both single and double row round hole injection, the film effectiveness increased with the blowing ratio, though lift-off was indicated by the data. The ammonia and diazo technique was used by Friedrichs et al. (1995) to measure the turbine nozzle endwall film effectiveness distribution. The technique is based on an established surface flow visualization technique and makes use of the reaction between ammonia gas and the diazo surface coating. Using the mass transfer analogy, the distribution of film cooling effectiveness on the endwall surface was determined. A similar method was used by Haslinger and Hennecke (1996) to obtain film effectiveness on a flat plate through single row injection.

Pressure sensitive paint (PSP), a relatively new technology, is already well-established and is widely used in the aerospace industry to measure the surface pressure (Mach number) distribution (Morris et al., 1992, Crites, 1993 and Lepicovsky, 1998). Zhang and Fox (1999) utilized the oxygen concentration sensitivity of PSP to measure the film effectiveness on a flat plate. Nitrogen gas was used as the film cooling flow as well as a tracer gas. The oxygen concentration of the mixture downstream from the injection was measured by the PSP. Film effectiveness was obtained by the heat and mass transfer analogy. Test results were compared with the traditional gas chromatography method. The PSP method to obtain film effectiveness was validated and the test data indicated that the method had higher potential due to its better spatial resolution, two-dimensionality and easy of use.

In this paper, film effectiveness results on a turbine nozzle surface are reported using the PSP technique. The tests were performed in a high speed turbine nozzle linear cascade, which correctly simulates engine operating conditions such as Reynolds number, Mach number and turbulence intensity. There are seven rows of film cooling holes on the nozzle surfaces. Only the data for injection from a suction surface single row of shaped holes are presented. Three blowing ratios were tested for each of the five freestream conditions: a reference condition, an increased and a reduced Reynolds number condition, and an increased and reduced Mach number condition.

The main objectives of this study are summarized below:

1. To measure film cooling effectiveness on turbine nozzle suction surface with single row injection using the PSP technique.
2. To study the effects of blowing ratio and freestream Reynolds and Mach numbers on the suction surface film effectiveness distribution.

TEST FACILITY AND INSTRUMENTATION

The tests were performed in the high speed wind tunnel apparatus as shown in Figure 1. The high speed warm cascade test facility was discussed by Zhang and Fox (1999). The mainstream air is filtered and pressurized by a four-stage centrifugal compressor, which is mounted on the roof. The compressed air goes through a control valve that can divert the flow to the exhaust and divert it back in the transient mode. It then passes through a venturi meter, a flow straightener, a converging nozzle and into a rectangular duct before it goes to the linear cascade test section. A turbulence grid is installed between the converging nozzle and the rectangular duct, which resulted in a turbulence intensity (Tu) of about 12.0% at the nozzle cascade inlet, as measured by a hot-film anemometer. The turbulence integral length scale (Λ_t) was 5.33 cm and energy length scale (Λ_e) was 14.3 cm.

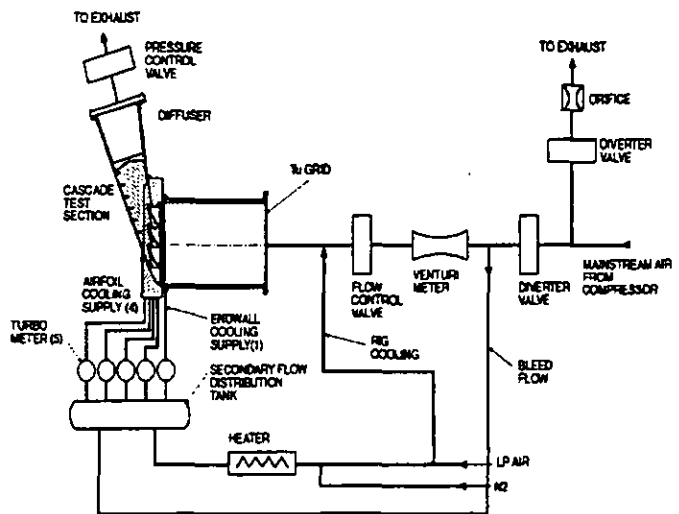


Figure 1. Schematic of Scaled Cascade Test Rig.

Based on turbulence measurements performed in a high pressure turbine (Zhang and Glezer, 1995), a 12.0% turbulence intensity is representative for a turbine nozzle inlet. (The effect of freestream turbulence on film cooling distribution is not studied in this paper.) The cascade test section is made of stainless steel, with transparent windows located on the top and one side of the cascade, to view the suction surface of the nozzle airfoils. The airfoil resembles that of a newly developed industrial gas turbine first-stage turbine nozzle. The

linear cascade consists of three airfoils and two curved sidewalls, for a total of four flow passages. The top endwall is flat and the bottom endwall is contoured, which resembles the actual engine geometry. There are four transparent windows on the rectangular duct to view the pressure surface, leading edge and part of the suction surface of the instrumented airfoils. Downstream from the cascade, the flow passes through a diffuser and a control valve and is discharged through an exhaust.

Table 1. Freestream Flow Conditions.

Condition	V_1 , m/s	Ma_1	Re_1	P_{1b} , mPa	Ma_2
Reference	37.7	0.11	283,000	0.119	0.72
Increased Ma	45.1	0.121	283,000	0.121	0.792
Decrease Ma	33.9	0.10	283,000	0.148	0.648
Increased Re	37.7	0.11	311,000	0.148	0.72
Decreased Re	37.7	0.11	255,000	0.121	0.72

The mainstream flow rate can be as high as 4 kg/s and the pressure as high as 0.16 mPa. The temperature of compressed air is about 350°K. The freestream flow conditions that simulate various Re and Ma numbers are listed in Table 1. The rig was validated by extensive flow measurements which include inlet/exist flow condition, airfoil surface pressure/Mach number measurements, periodicity, and turbulence intensity and length scale. Some of the flow measurement results will be discussed in a later section.

The instrumented two time linear size nozzle along with film cooling holes are shown in Figure 2. It was based on a current mid-size industrial gas turbine stage one nozzle design, which has a four row shower head arrangement, a single row of round holes on the pressure surface and two rows of shaped holes on the suction surface. In this paper, only the data for injection from the second row on the suction surface was presented.

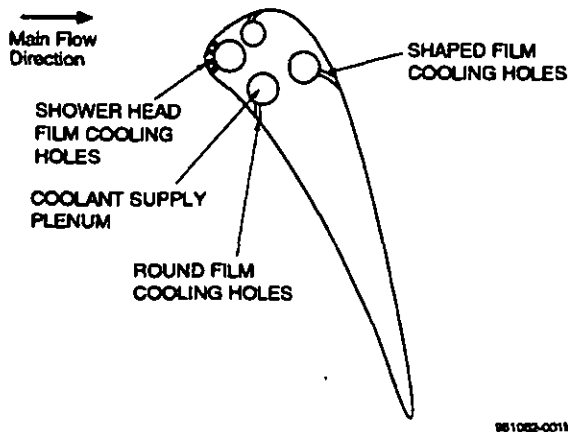


Figure 2. Film Cooling Instrumented Vane - Reference Geometry.

There are 13 shaped film cooling holes with a diameter of 1.12 mm. The hole pitch is 3.8 mm, resulting in a P/D of 3.4. The length of the hole is about 3.5 times the hole diameter. The shaped exit starts at 1.75 P/D with a 10° spanwise expansion on both sides and a 10° layback on the streamwise direction. The hole has an injection (streamwise) angle of 35° and no compound (spanwise) angle. Nitrogen gas or compressed air was used for the film cooling flow and was supplied by pipelines. It was introduced through a pressure regulator, a heater, and turbo meters and then was brought into four distribution plenums, a shower head plenum, a forward suction surface plenum, a backward suction surface plenum, and a pressure surface plenum. Each plenum is individually controlled and monitored by an Allen Bradley PLC-5 programmable controller by turbo meters. Pressure taps and thermocouples were mounted in each of the plenums to measure and to control the cooling air/nitrogen supply temperatures and pressures. To reduce the heat losses through the plumbing, rubber heaters were used to maintain the temperature of the pipes and flow meters. The temperature difference between the mainflow and the secondary flow can be kept below 0.5°K.

EXPERIMENTAL TECHNIQUE AND DATA REDUCTION OF PRESSURE SENSITIVE PAINT (PSP)

PSP techniques are based on oxygen quenched photoluminescence. Photoluminescence is the property of some compounds (active part of PSP) to emit light after being illuminated by a suitable light source. The intensity of the emitted light depends on the oxygen partial pressure and directly relates to the pressure of a surrounding gas which contains oxygen. In this study, 450 nm light was used to excite the active molecules with the return signal in the 600 nm wavelength. To detect and record the emitted light, which contains both pressure and concentration information, a filter and a CCD camera were used. A data reduction program was used to analyze the data. In addition to measuring the static pressure distribution on the test surface, this oxygen sensitivity is used to indicate the oxygen concentration in the gas mixture. Nitrogen gas was heated to the temperature of the freestream to eliminate any temperature effect. It was then injected through the film cooling holes into the main flow. The mass concentration of the nitrogen/air mixture downstream from the point of injection can be measured to obtain film effectiveness using the so-called mass transfer analogy. The mass fraction of the tracer gas in the mixture near the wall surface is related to the adiabatic wall temperature for the analogous heat transfer situation. In the current study, the mainstream contained approximately 79% nitrogen and the cooling flow contained approximately 100% nitrogen. The film effectiveness can be expressed by oxygen concentrations, which can be measured by the PSP:

$$\eta = \frac{C_{\infty} - C_{mix}}{C_{\infty}} \quad (2)$$

where C_{∞} is the oxygen concentration of the mainstream (about 21%) and C_{mix} is the oxygen concentration of the air/nitrogen mixture (between 0 to 21%). Hence, the film effectiveness is between 0% (far downstream) and 100% (inside the hole).

A test setup of the PSP application to obtain film effectiveness includes a test vane, a CCD camera and light sources. The test vane was made of stainless steel and was coated with PSP, which can be mounted at the middle (for viewing the leading edge and the suction surface) or at the mid-left position in the five vane cascade.

Transparent windows were located immediately in front and downstream of the cascade. The CCD camera was mounted in front of these windows to view the vane surfaces from four positions: two for viewing the pressure surface, one for viewing the leading edge, and one for viewing the suction surface. In this study, only the suction surface view was used. Three halogen lamps were located around the camera to provide light sources. Figure 3 shows the setup for the PSP film cooling measurement viewing the suction surface. The images of luminescence intensity distribution from the nozzle surfaces, recorded by the CCD camera, were originally gray scaled. These images were saved as .tif files and then calculated by the data reduction program which compared ratios of the recorded intensity values with the calibration data to obtain the surface pressure and film effectiveness distributions. For the PSP film cooling test, four images were required: a dark image (light off, wind off), a reference image (wind off, light on), an air injection image (wind on, light on, hot air injection), and a nitrogen injection image (wind on, light on, hot nitrogen injection). The air injection image is necessary to eliminate the effect of surface pressure variation. Hot means the temperature of the mainstream, about 350°K, and cold means the reference temperature, controlled at 294°K.

An uncertainty analysis was performed on the film effectiveness measurement using the PSP based on the method by Kline and McClintock (1953). The uncertainty of the pressure distribution was 5.8% and the uncertainty of film effectiveness at the nominal condition was 12.0%. The net film effectiveness variation ($\Delta\eta$) was 0.06 for the worst case.

PSP CALIBRATION

The PSP was calibrated regularly before testing. A sample coupon made of copper and coated with PSP was used for the calibration. Three thermocouples were installed underneath the front surface of the coupon to measure the surface temperature. The sample coupon was located inside a pressure chamber which was connected to both a vacuum pump and a compressed air source. A heater, located in close contact to the back side of the sample coupon, heated the coupon surface to the desired temperature with an accuracy of less than 0.5°K. The camera was mounted in front of a transparent



Figure 3. PSP Test Setup - Viewing the Suction Surface from Downstream of the Cascade.

window facing the sample coupon. Two halogen lamps with filters were located on both the left and right sides of the camera. Since the

cascade rig operation was at a pressure of approximately 136 kPa at the cascade inlet and at a temperature of approximately 350°K, the PSP was calibrated to a temperature between 344°K and 356°K and pressure from vacuum to 150 kPa. Atmospheric pressure was used as a reference pressure for each of the calibrated temperatures. The results are presented as the reverse intensity ratio to the pressure ratio and were curve fitted and stored in the data reduction program which can automatically adjust temperature if the test temperature varied from the reference temperature.

FLOW MEASUREMENT RESULTS

To meet the critical flow condition requirements and to guarantee a correct simulation of the engine operating parameters in the cascade, extensive flow measurements were performed before heat transfer and film cooling testing was initiated. At the inlet of the cascade, mean velocity, turbulence intensity and turbulence length scale were surveyed horizontally and vertically across the rectangular duct, using the hot-film anemometer and surface pressure taps. Flow uniformity and periodicity were achieved at the inlet. At the exit of the cascade, although a great effort was made, flow uniformity and periodicity were not attained due to an uneven diffusion effect of the downstream side walls. Surface Mach number measurements were performed for various freestream conditions at all three airfoil locations. The results directly correspond to exit Mach number measurements. Without a tail board, a correct simulation of surface Mach number can only be achieved in the mid-left flow passage, which is a combination of the suction surface of the middle airfoil and the pressure surface of the mid-left airfoil as viewed from the cascade inlet. Figure 4 shows the pressure tap locations on the instrumented airfoil which were used to measure the airfoil surface static pressure. There are 12 pressure taps on the pressure surface and 15 on the suction surface, all located at the mid-span position. Figure 5 shows the measured surface Mach number distributions from the mid-left flow passage for the five freestream conditions studied. The Mach number distributions for the reference flow condition and increased and reduced Reynolds number conditions collapse into one line and match the CFD prediction by the Dawes code. The Mach number distributions for the Mach number increased and reduced flow conditions lie above and below the respective CFD prediction.

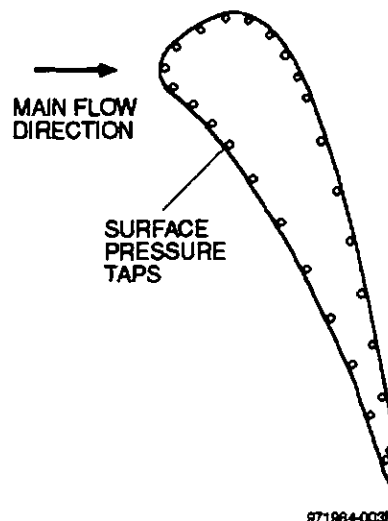


Figure 4. Pressure Tap Locations on the Instrumented Nozzle Airfoil.

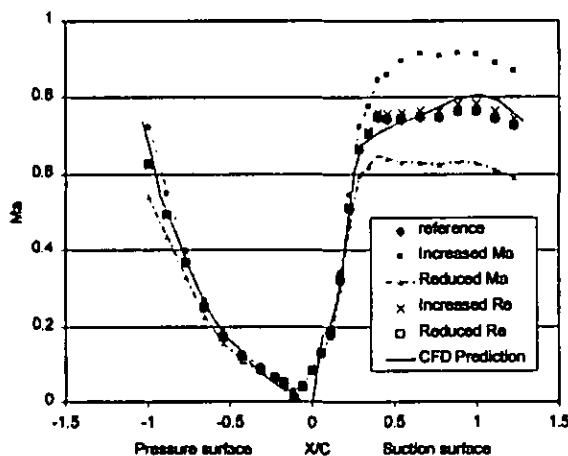


Figure 5. Surface Mach Number Distributions for the Five Mainstream Flow Conditions.

FILM EFFECTIVENESS MEASUREMENTS RESULTS

Repeatability tests were performed to validate the PSP technique, particularly for the film injection presented in this paper. If the same (PSP) paint and same painting process are used, as the tests performed in this paper, the difference in average film effectiveness is less than 2%. If different paint or different painting processes are used, the difference of film effectiveness for different tests can reach 4%. For each of the freestream flow conditions, film effectiveness was measured at three blowing ratios, $M = 0.5$, 1.0 and 1.5, defined based on coolant and local freestream parameters, representative of typical cooling designs. The film cooling holes in this study are located at an X/C of 0.34, just upstream of the nozzle throat. The injection is followed by a mild acceleration, a fairly stable velocity region and a mild deceleration (Figure 5).

Effect of Blowing Ratio

The experimental results of film effectiveness distributions for blowing ratios 0.5, 1.0 and 1.5 using the PSP method are shown in Figure 6. A qualitative evaluation of the results indicated that there is a considerable uneven cooling flow distribution among the cooling holes. This is a result of the uncertainty of the manufacturing process (EDM). The length for each of the cylindrical part of the holes is not the same, causing a difference in discharge coefficient. As a result the film effectiveness is not evenly distributed among the holes. At a blowing ratio of 0.5, the film cooling jets were attached to the suction surface. At the center lines downstream of the injection, a high film effectiveness was observed. Between the holes near the point of injection, the film effectiveness was low, about 0.1, while the film effectiveness at the center line downstream of the injection was quite high. This indicated that the jet flow was comparatively attached to the surface. Although the freestream turbulence intensity was about 12.0% at the cascade inlet, the local turbulence intensity near the suction surface could be much lower due to acceleration and high mean velocity. This kind of turbulence feature cannot be reproduced in a low speed wind tunnel. The spanwise average film effectiveness decayed quickly to about 0.1 at an X/D close to 25. At a blowing ratio of 1.0, the difference in film effectiveness between the center line and the line between holes became smaller. This indicated that the mixing between the film jet and the freestream was enhanced, but no film jet lift-off was observed. This trend of film effectiveness improving with

the blowing ratio continued up to a blowing ratio of 1.5. Close to the trailing edge, the average film effectiveness is about 0.2. The effect of

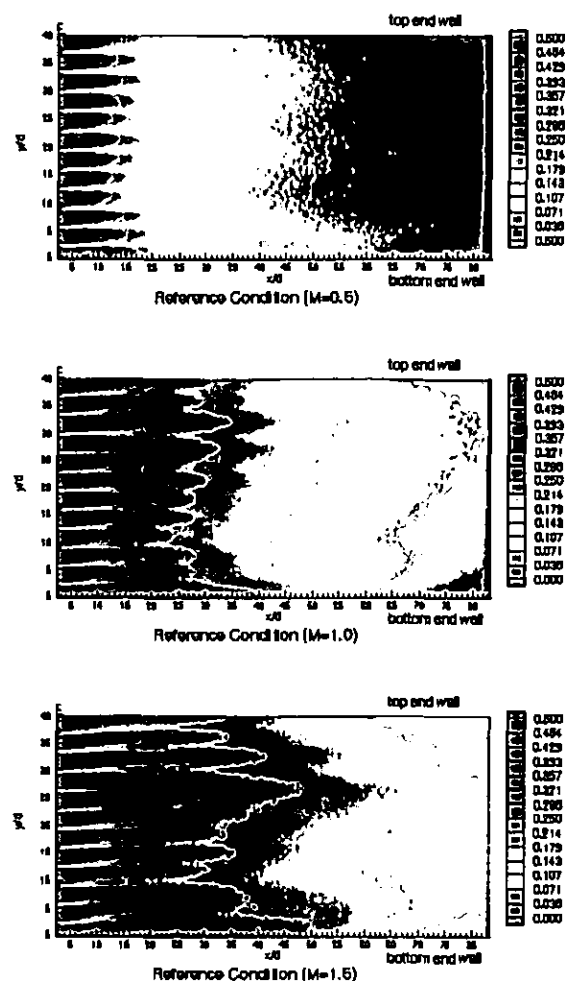


Figure 6. Film Effectiveness Distributions on the Suction Side - Effect of Blowing Ratio.

secondary flow on suction surface film coverage is also demonstrated by the results for blowing ratios of 1.0 and 1.5. The film effectiveness decreased quickly closer to an endwall as compared to that at the mid span, swiped away by the up-wash passage vortex. As a result, two triangular regions were formed near the trailing edge and the endwall corner where the film effectiveness was almost zero.

Figure 7 shows the average and center line film effectiveness distributions for the reference flow condition. As a comparison, film effectiveness results measured by Giebert et al. (1997) and Ames (1997b) are plotted in the average distribution figure. Current film effectiveness distributions lie slightly below those by Giebert et al. and Ames. At a blowing ratio of 0.5, both the average and center line film effectiveness decreased quickly downstream of the injection. At an X/D of about 25, there was essentially no difference between the average and center-line values. There was a significant increase in film effectiveness, however, when the blowing ratio was increased to 1.0. From $X/D = 20$ to the trailing edge, the film effectiveness values were almost double those of $M=0.5$. When the blowing ratio increased to 1.5, both the average and center line effectiveness was lower close to the injection point than those for $M=1.0$, an indication

of partial separation of the film jets from the wall (lift-off). Downstream of $X/D=10$, the effectiveness curves are higher than that of $M=1.0$ due to the reattachment of the film jets to the surface. Considering that the coolant mass flow rate was proportional to the blowing ratio, the increase in film effectiveness value from $M=1.0$ to $M=1.5$ was not as significant as that from $M=0.5$ to $M=1.0$ until near the trailing edge, where the effectiveness was almost directly proportional to the introduced cooling mass flow.

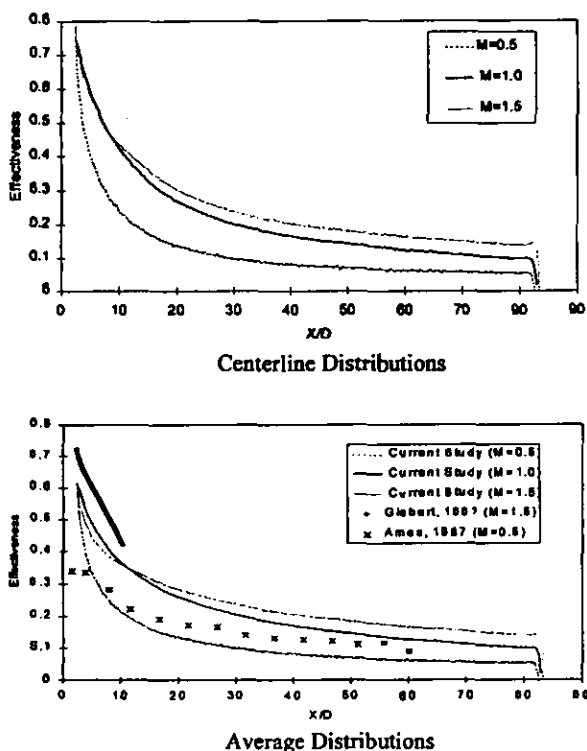


Figure 7. Center Line and Average Film Effectiveness Distributions – Effect of Blowing Ratio.

Figure 8 shows the spanwise film effectiveness distributions at two X/D locations. The flow rate between the film holes was not evenly distributed due to the manufacturing uncertainty. But the secondary flow effect on the suction surface film cooling is clearly indicated by the results at $X/D=70$, including that for $M=0.5$ which is not as clearly seen in Figure 6.

Effect of Freestream Re Number

The film effectiveness distributions for three Reynolds numbers and a blowing ratio of 1.0 are shown in Figure 9. All three Reynolds numbers were controlled by changing both the mainstream and film cooling flow densities to maintain the freestream Mach number at the same value. The reason for a lower film effectiveness at a higher Reynolds number is probably due to a higher density of both the

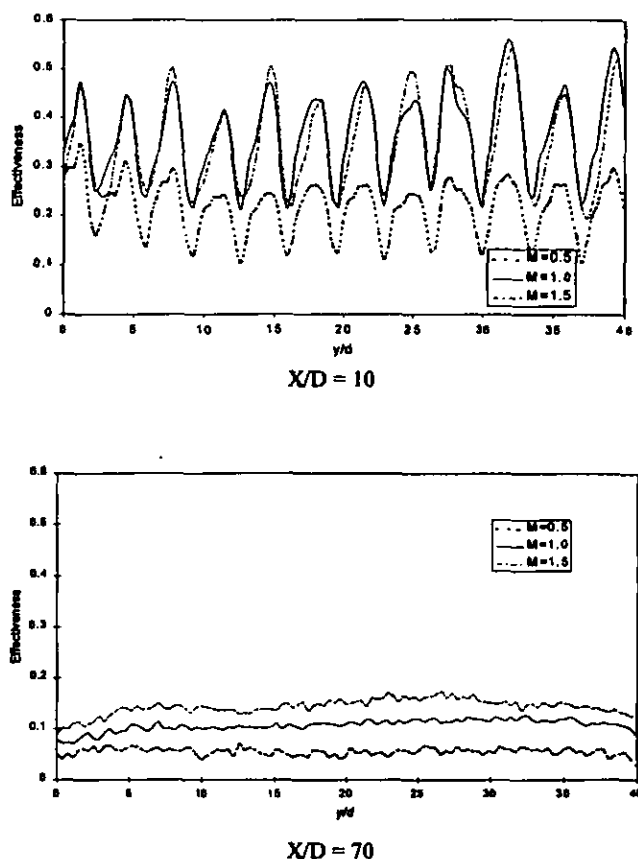


Figure 8. Spanwise Film Effectiveness Distributions at Various X/D Locations – Effect of Blowing Ratio.

mainstream and the film jets, resulting in a higher momentum exchange between the film jets and the mainflow. The location of the film injection also played an important role in the density dependence of the film coverage. The film cooling holes are located at the mid-chord on the suction surface, where a turbulent boundary layer is more likely to be developed. Higher density enhances turbulent momentum exchange in the turbulent boundary layer. The effect of the secondary flow on the film effectiveness was enhanced by a higher Reynolds number, particularly near the curved endwall (bottom endwall).

Figure 10 shows the average film effectiveness distributions for three Reynolds number conditions and three blowing ratios. At a blowing ratio of 0.5, the average film effectiveness distribution for the reference freestream condition lies between that for the reduced Reynolds and increased Reynolds number conditions. The difference between the increased Reynolds

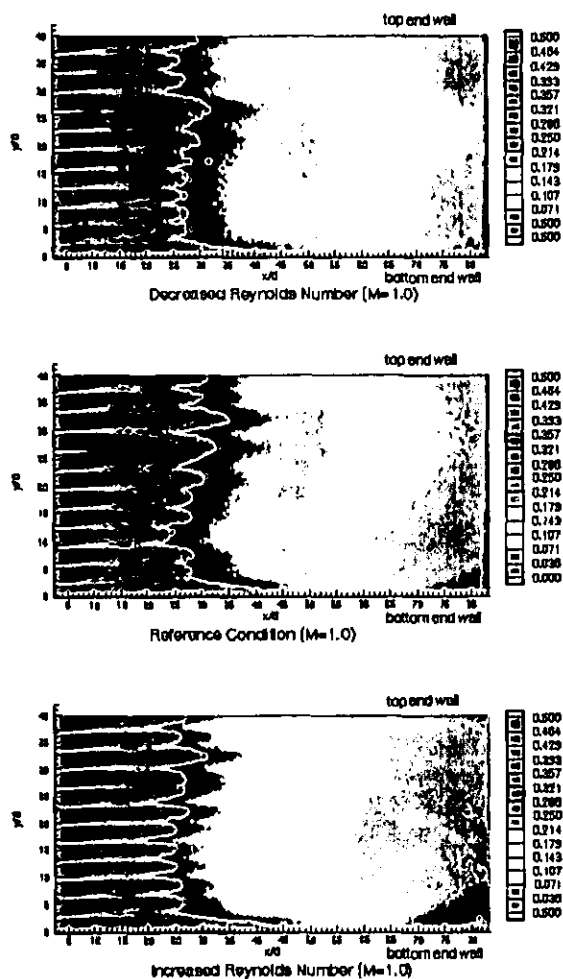


Figure 9. Film Effectiveness Distributions – Effect of Re Number, $M=1.0$.

number condition and the reference condition was more pronounced than those between the reference and the decreased Reynolds number conditions. When the blowing ratio is increased to 1.0, the average film effectiveness distributions for the reduced Reynolds number and for the reference conditions collapse into one line, while the distribution for the increased Reynolds number condition lies considerably below them, although not as significant as that for $M=0.5$. At $M=1.5$, the average film effectiveness distributions for three Reynolds number conditions collapse into one curve. This indicated that the film effectiveness on the suction surface through shaped hole injection is no longer dependent on the freestream Reynolds number when the blowing ratio is high.

Effect of Freestream Mach Number

The experimental results of film effectiveness distributions for the three Mach numbers and for a blowing ratio of 1.0 are shown in Figure 11. In a qualitative sense, the film effectiveness was higher for the reference flow condition than for both the increased and decreased Mach conditions. All three Mach numbers were controlled by simultaneously changing the mainstream density and velocity to keep a constant freestream Reynolds number. A lower film effectiveness at lower Mach number was expected due to the density effect which was partially supported by the test results at the reduced Mach condition.

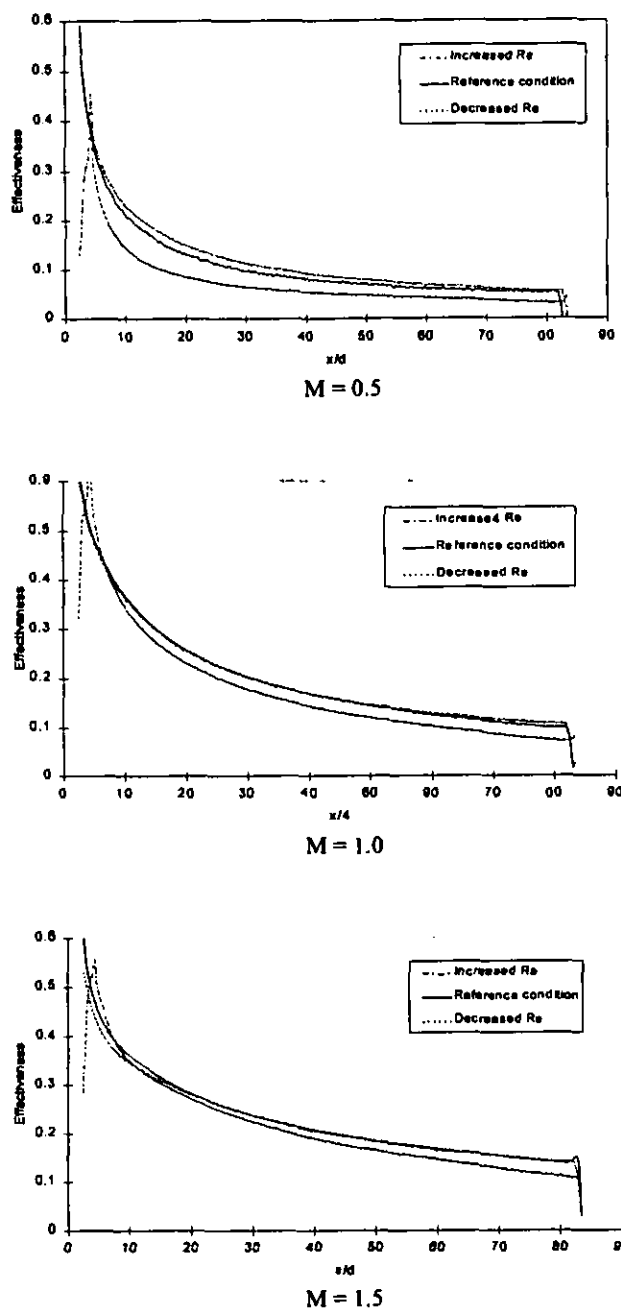


Figure 10. Average Film Effectiveness Distributions – Effect of Reynolds Number.

At the increased Mach number condition, the effectiveness was lower than that for the reference condition. This is considered to be due to the fact that the film holes were located directly upstream of the nozzle throat. At the higher Mach number condition, the Mach number near the throat was close to one. The film jets could be partially damaged by an unsteady shifting of the local Mach number from one to less than one. The film effectiveness is sensitive to the mainstream acceleration which is related to the Mach number change upstream and downstream of the injection, as can be seen in Figure 5. A small change results in a significant change in acceleration near the

injection. Considering the effect of the secondary flow on the film effectiveness, it is stronger at a lower Mach number due to a higher freestream density, which is consistent with varying the Reynolds number cases.

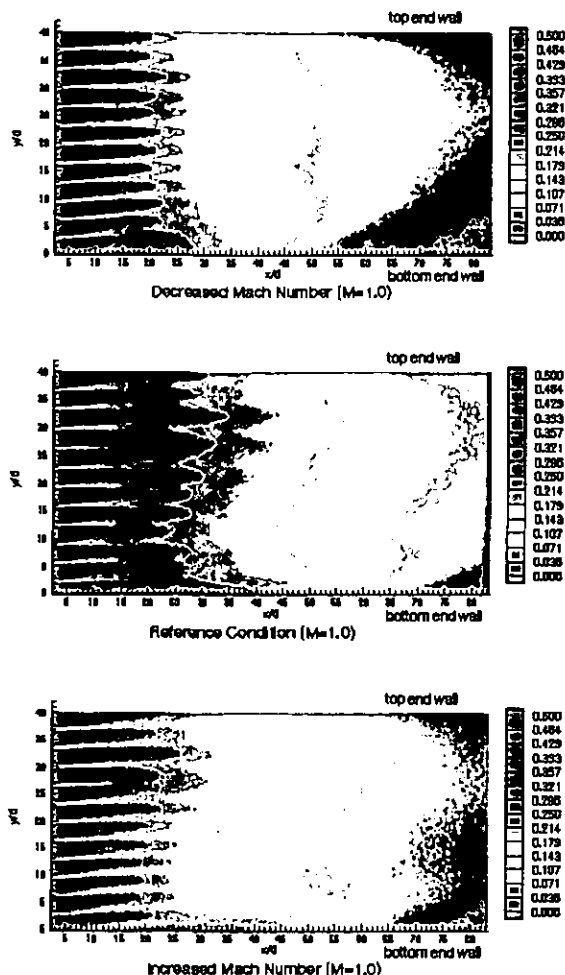


Figure 11. Film Effectiveness Distributions – Effect of Mach Number, $M=1.0$.

Considering the Mach number effect on the average film effectiveness distribution in Figure 12, at a blowing ratio of 0.5, the average film effectiveness distribution of the reference freestream condition lies significantly above that of the decreased and increased Mach flow conditions. Downstream of the injection, the reduction of average effectiveness by increasing and decreasing the Mach number was about 40% of that at the reference condition. The difference of the average film effectiveness between the increased Mach number and reduced Mach number conditions was quite small. As the blowing ratio increased to 1.0, the average film effectiveness distributions of the decreased and increased Mach number conditions collapsed into one line downstream of $X/D=20$ and both lie significantly below that of the reference condition. From the injection point to $X/D=20$, where the nozzle throat is located, the distribution of the increased Mach number lies below those for the decreased Mach number. At $M=1.5$, the average film effectiveness distributions of the increased and reduced Mach number conditions lie below and above, respectively, that of the reference condition upstream of $X/D=25$ and both lie below that of the reference condition downstream from $X/D=25$. The better film

coverage near the injection for the reduced Mach number condition could probably be explained by the higher density which helps the mixing of the film jets with the mainstream.

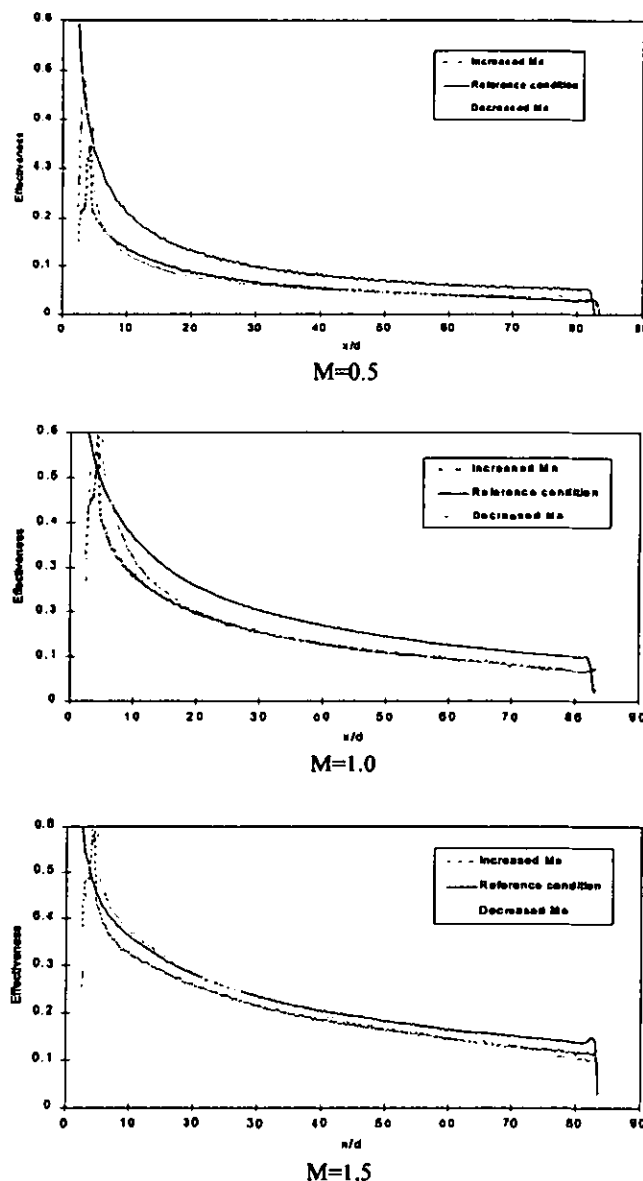


Figure 12. Average Film Effectiveness Distributions – Effect of Mach Number.

CONCLUSIONS

The film effectiveness was measured on the suction surface of a high pressure gas turbine nozzle surface using the PSP technique and the mass transfer analogy. The main conclusions were:

1. For suction surface shaped hole injection, the film effectiveness increased with the blowing ratio from $M=0.5$ to 1.5. At $M=1.5$, a partial lift-off was indicated by the results, while the downstream film effectiveness was high.
2. Even though the freestream turbulence is 12.0% at the nozzle inlet, a significant spanwise variation of the film

- effectiveness was observed due to the effect of the secondary flow, uneven distribution of the cooling film and insufficient mixing on the suction surface.
3. The film effectiveness on the suction surface shaped-hole injection was affected by the freestream Reynolds number and decreased with an increase in Reynolds number. The effect was less pronounced at a higher blowing ratio.
 4. The film effectiveness on the suction surface shaped-hole injection decreases with a decrease in Mach number. When the nozzle throat Mach number was near one, the film coverage was also reduced. The effect was less pronounced at a higher blowing ratio.

ACKNOWLEDGMENTS

The work presented in this paper was performed as a part of the Advanced Turbine Systems Technology Development Program, sponsored both by the U.S. Department of Energy and Solar Turbines Incorporated. The authors of this paper also want to acknowledge the contribution of Dr. Boris Glezer (Head of Solar Turbines Cooling Design and Analysis), who recommended the use of PSP in cooling effectiveness studies.

REFERENCES

- Ames, F. E., 1997a, "Aspects of Vane Film Cooling with High Turbulence: Part I - Heat Transfer," ASME, 97-GT-239.
- Ames, F. E., 1997b, "Aspects of Vane Film Cooling with High Turbulence: Part II - Adiabatic Effectiveness," ASME, 97-GT-240.
- Abuaf, N., Bunker, R., and Lee, C. P., 1995, "Heat Transfer and Film Cooling Effectiveness in a Linear Airfoil Cascade," ASME, 95-GT-3.
- Cites, R. C., 1993, "Experience Using Pressure Sensitive Paint in NASA Lewis Research Center Propulsion Test Facilities," AIAA, 95-2831.
- Du, H., Han, J. C., and Ekkad, S. V., 1997, "Effect of Unsteady Wake on Detailed Heat Transfer Coefficient and Film Effectiveness Distributions for a Gas Turbine Blade," ASME, 97-GT-166.
- Drost, U. and Böles, A., 1998, "Investigation of Detailed Film Cooling Effectiveness and Heat Transfer Distributions on a Gas Turbine Airfoil," ASME, 98-GT-20.
- Friedrichs, S., Hodson, H. P., and Dawes, W. N., 1995, "Distribution of Film Cooling Effectiveness on a Turbine Endwall Measured Using the Ammonia and Diazo Technique," ASME, 95-GT-1.
- Giebert, D., Gritsch, M., Schulz, A., and Wittig, S., 1997, "Film-cooling from Holes with Expanded Exit: A Comparison of Computational Results with Experiments," ASME, 97-GT-163.
- Goldstein, R. J., 1971, "Film Cooling," Advances in Heat Transfer, Academic Press, New York, Vol. 7, pp. 321-379.
- Haslinger, W. and Hennecke, D. K., 1996, "The Ammonia and Diazo Technique with CO₂-Calibration for Highly Resolving and Accurate Application to a Row of Holes," ASME, 96-GT-438.
- Kline, S. J. and McIntock, F. A., 1953, "Describing Uncertainties in Single Sample Experiments," Mechanical Engineering, vol. 75.
- Lepicovsky, J., 1998, "PSP Measurement of Stator Vane Pressure in a High Speed Fan," ASME, 98-GT-499.
- Morris, M. J., Donovan, J. F., Kegelmann, J. T., Schwab, S. D., Levy, R. L., and Crites, R. C., 1992, "Aerodynamic Application of Pressure Sensitive Paint," AIAA, 92-0264.
- Pedersen, D. R., Eckert, E.R.G. and Goldstein, R. J., 1977, "Film Cooling with Large Density Differences Between the Mainstream and the Secondary Fluid Measured by the Heat-Mass Transfer Analogy," ASME Journal of Heat Transfer, Vol. 99, pp. 620-627.
- Takeishi, K., Matsuura, M., Aoki, T., and Sato, T., 1989, "An Experimental Study of Heat Transfer and Film Cooling on Low Aspect Ratio Turbine Nozzles," ASME, 89-GT-187.
- Takeishi, K., Aoki, T., and Sato, T., 1991, "Film Cooling on a Gas Turbine Rotor Blade," ASME, 91-GT-279.
- Vendula, R. J. and Metzger, D. E., 1991, "A Method for Simultaneous Determination of Local Effectiveness and Heat Transfer Distributions in Three-Temperature Convection Situations," ASME, 91-GT-345.
- Wang, Z., Ireland, P. T. and Jones, T. V., 1994, "A Color Image Processing System for Transient Liquid Crystal Heat Transfer Experiments," ASME, 94-GT-290.
- Zhang, L. J. and Fox, M., 1999, "Flat Plate Film Cooling Measurement Using PSP and Gas Chromatography Techniques," Fifth ASME/JSME Joint Thermal Engineering Conference, San Diego, CA.
- Zhang, L. J. and Glezer, B., 1995, "Indirect Turbulence Measurement in Gas Turbine Stages Using Heat Flux Probe," ASME, 95-GT-153.